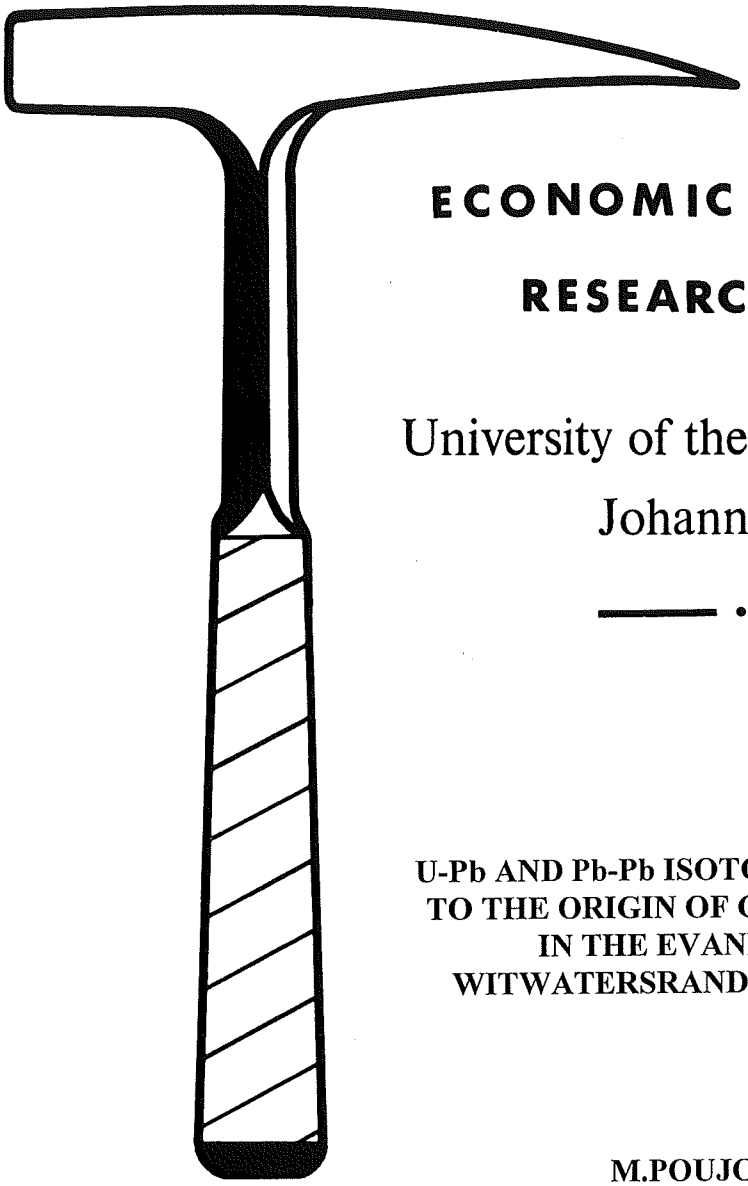

ECONOMIC GEOLOGY

RESEARCH UNIT

University of the Witwatersrand

Johannesburg

U-Pb AND Pb-Pb ISOTOPIC STUDIES RELATING TO THE ORIGIN OF GOLD MINERALIZATION IN THE EVANDER GOLDFIELD, WITWATERSRAND BASIN, SOUTH AFRICA

M.POUJOL, L.J.ROBB and J.P RESPAUT

INFORMATION CIRCULAR No. 320

UNIVERSITY OF THE WITWATERSRAND
JOHANNESBURG

U-Pb AND Pb-Pb ISOTOPIC STUDIES RELATING TO THE ORIGIN OF GOLD MINERALIZATION IN THE EVANDER GOLDFIELD, WITWATERSRAND BASIN, SOUTH AFRICA

by

M. POUJOL[1], L.J. ROBB[2] and J.P RESPAUT[1]
([1] UMR 5567 CNRS/UM2, ISTEEM, cc066, Université Montpellier II,
34 095 Montpellier Cedex 5, France
[2]Department of Geology, University of the Witwatersrand,
P/Bag 3, WITS 2050, South Africa)

ECONOMIC GEOLOGY RESEARCH UNIT
INFORMATION CIRCULAR No. 320

March, 1998

U-Pb AND Pb-Pb ISOTOPIC STUDIES RELATING TO THE ORIGIN OF GOLD MINERALIZATION IN THE EVANDER GOLDFIELD, WITWATERSRAND BASIN, SOUTH AFRICA

ABSTRACT

Studies of the detrital components from the conglomerate horizons within the major goldfields of the Witwatersrand Basin, South Africa, indicate a mixed granite-greenstone source of two distinct ages, and a deposition interval between 3074 Ma and 2714 Ma. This study presents new U-Pb and Pb-Pb isotopic data for the Central Rand Group from the Evander Goldfield, located in the eastern extremity of the Witwatersrand Basin where no previous isotopic data has been derived. Single detrital zircon dating exhibits a more restricted range of ages than previously published data from the other goldfields, and a shift towards younger ages. The oldest grain measured is ca. 3180 Ma, while the majority of detritus falls in the range 3050-2850 Ma, with a mean age at ca. 2960 Ma. In addition, however, several zircon grains from shear zones and altered portions of the Kimberley Reef, yield ages that are younger or similar to that of the Ventersdorp lavas. These ages are attributed to partial or complete isotopic resetting of older detritus at some stage during the post-depositional history of the Basin.

The existence of detrital as well as authigenic pyrite is also supported by the present study. A small proportion of the pyrite, mainly extracted from unaltered sediments in the Kimberley Reef footwall, yield ages that are in excess of the minimum depositional age of the Witwatersrand Basin. Authigenic pyrite, as well as detrital grains from highly altered portions of the Kimberley Reef define secondary isochrons at 2370 Ma and 2020 Ma, ages that accord with the resetting signatures from zircon in the present study and pyrite analysed in previous studies. The lead isotopic signature of the 2370 Ma event is probably associated with burial of the Witwatersrand Basin by the upper portion of the Transvaal Supergroup, and suggests circulation of highly radiogenic fluids at this time. Isotopic signatures for the 2020 Ma event are probably related to intrusion of the Bushveld Complex and/or Vredefort catastrophism, and appear to be associated with a fluid that was less radiogenic. The present study, which combines single grain U-Pb dating of the zircon with Pb-Pb studies of sulphide phases in the Evander Goldfield, has produced a number of new results which support a complex, polyphase evolution and genesis of the Au-U deposits within the Witwatersrand Basin.

__oOo__

U-Pb AND Pb-Pb ISOTOPIC STUDIES RELATING TO THE ORIGIN OF GOLD MINERALIZATION IN THE EVANDER GOLDFIELD, WITWATERSRAND BASIN, SOUTH AFRICA

CONTENTS

	Page
INTRODUCTION	1
GEOLOGICAL SETTING	1
Witwatersrand Basin	1
Evander Goldfield	3
SAMPLING	4
ANALYTICAL METHODS	5
Single Zircon Grain Analysis	5
Pyrite Analysis	5
RESULTS	5
U-Pb Isotopic Data on Zircon Grains	5
Detrital Zircon Grains	6
Younger Zircons of Uncertain Origin	8
Pyrite	10
CONCLUSIONS	14
REFERENCES	15

__oOo__

Published by the Economic Geology Research Unit
Department of Geology
University of the Witwatersrand
1 Jan Smuts Avenue
Johannesburg 2001
South Africa

ISBN 1-86838-204-4

INTRODUCTION

In 1886, George Harrison discovered gold in conglomerate on the northern slope of the Witwatersrand range (Antrobus, 1986). Today, the 3074-2714 Ma Witwatersrand Basin (Fig.1) is amongst the best-studied of Archaean sedimentary basins and constitutes one of the largest gold producing regions of the world. For these reasons, the Basin has been the subject of intensive studies which are often marked by continuing controversy between modified placer and hydrothermal models for the origin of mineralization (Skinner and Merewether, 1986; Pretorius, 1991). Detrital components are described as coming from a mixed granite-greenstone source of two distinct ages (Wronkiewicz and Condie, 1987 ; Robb and Meyer, 1994); the one source comprises 3450-3250 Ma Barberton-type greenstone belts and granitoids > 3100 Ma in age, and the other consists of younger greenstone belts (such as the 3090-2970 Ma Murchison greenstone belt and possibly the Kraaipan Formation) and granitoids <3100 Ma in age.

With the advent of improved dating technology, provenance studies are now very often carried out by determining the ages of single zircon grains, which are a common accessory mineral within the Witwatersrand Basin . The identification of different age populations of such minerals would assist in better constraining the source of the sediments in the Basin, as well as the origin of detrital gold and uranium particles. Two studies of detrital zircons have already been published (Barton et al., 1989; Robb et al., 1990), mainly for conglomerate horizons along the northern, western and southern flanks of the Basin. There is, however, no data available for the eastern extremities of the Basin and the purpose of this paper is, therefore, to present new data for the Evander Goldfield (120 km east of Johannesburg) which is the easternmost region of the Witwatersrand Basin (Fig. 1). A U-Pb study on single abraded detrital zircons has been undertaken with a view to obtaining additional information on the sediment source for this portion of the Basin. Several different samples of the well-mineralized Kimberley Reef, as well as rock from the footwall and hangingwall successions, from the Kinross Mine, have been collected for this purpose. In addition, a Pb-Pb study on both detrital and authigenic pyrites found in these sediments was also undertaken in order to examine the nature and timing of post-depositional mineralization processes in the formation of the Witwatersrand Au-U deposits.

GEOLOGICAL SETTING

Witwatersrand Basin

Deposited on the Kaapvaal Craton (Fig. 1) in the late-Archaean, the Witwatersrand Basin is represented by a 5 to 8 km-thick succession of mainly clastic sediments which form part of the so-called Witwatersrand Triad (i.e. Dominion Group, Witwatersrand and Ventersdorp Supergroups) deposited between 3074 Ma and 2714 Ma. These sequences were successively deposited on a granitoid-greenstone Archaean basement , now partially exposed within the 3180 Ma Johannesburg Dome (Anhaeusser and Burger, 1982) on the northern flank of the Basin.

The tectonic setting of the Craton during Witwatersrand deposition has been summarized in a recent model which envisages the amalgamation of the entire Kaapvaal Craton in a series of accretionary events between ca. 3650 and 2700 Ma (De Wit et al., 1992). In this model, the craton is considered to be made up of a collage of subterranes each with distinct geological attributes. According to these authors, the formation of the Craton can be subdivided in two main periods: The first period between ca 3650 and 3100 Ma Ga is characterized by the initial separation of the continental crust from the mantle. The second period (3.1 to 2.7 Ga) records intra-continental and continental-margin processes, during which time the formation of the Witwatersrand Basin occurred.

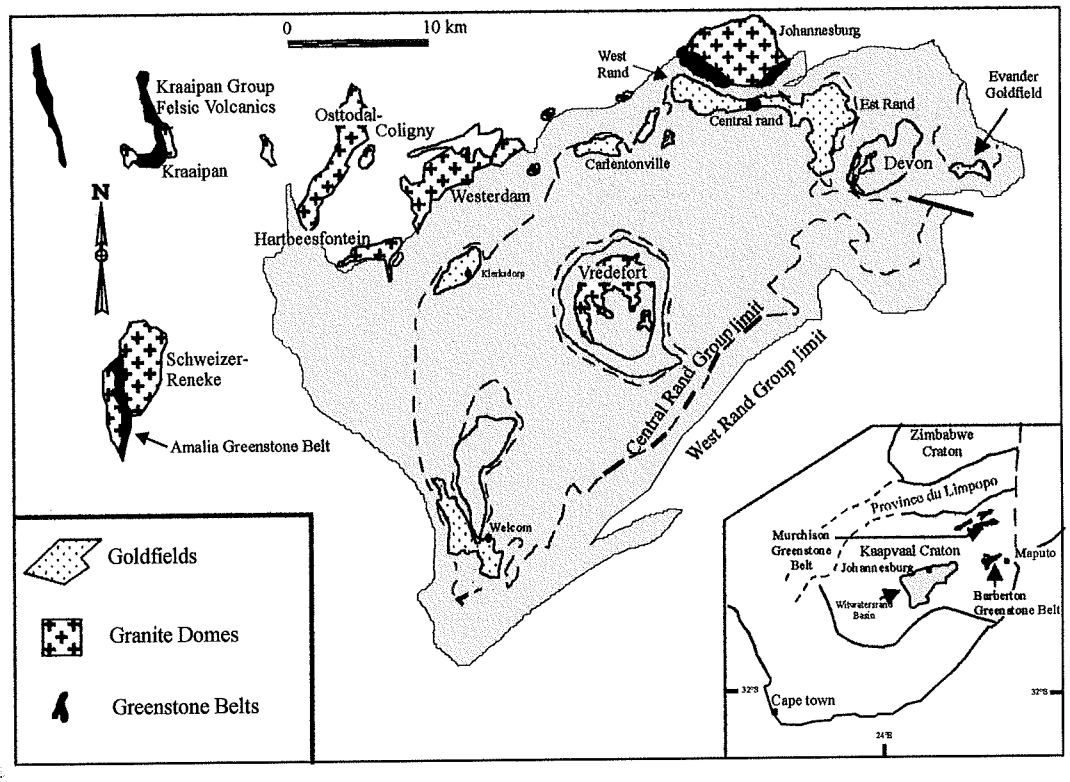

***Figure 1** : Simplified outline and locality map of the Witwatersrand Basin and surrounding Archaean granite-greenstone terrane(After Robb et al., 1990). Location of the Wiwatersrand Basin within the Kaapvaal Craton is shown in the inset map.*

The Witwatersrand Triad comprises three main components; the Dominion Group forms the base of the sequence and comprises a thin basal quartzite and conglomerate package overlain by bimodal, volcanic rocks. The overlying Witwatersrand Supergroup is subdivided in two main units; the lower West Rand Group which comprises essentially shales and quartz-arenites with only minor conglomerates, and the upper Central Rand Group dominated by quartz-wackes and quartz-arenites containing numerous intercalated conglomerate bands and only a minor shale component. The West Rand Group is considered to have been deposited during the interaction of marine shelf and tidal environments with river-dominated fan deltas (Watchorn and O'Brien, 1991). During the deposition of the Central Rand Group, the sediments were largely accumulated in shallow braided-stream environments (Minter, 1978). The sediment input vectors define a contiguous region to the north, northwest, west and southwest of the actual limits of the Basin as the provenance. The Witwatersrand Supergroup is itself overlain by mafic to ultramafic rocks and largely volcaniclastic sediments of the Ventersdorp Supergroup. Metamorphic conditions experienced by mineralized Witwatersrand conglomerates along the Basin margins have been estimated at upper greenschist facies with maximum temperatures of about 350°C and pressures of 2.5 to 3 kbars (Phillips, 1988; Wallmach and Meyer, 1990).

The economically viable ore-bearing reefs are almost entirely contained within the Central Rand Group. At least five types of gold have been described from within the Witwatersrand Basin (Hallbauer, 1986): (1) detrital gold particles; (2) authigenic gold associated with carbonaceous matter; (3) authigenic gold reconstituted by metamorphic or diagenetic processes; (4) primary gold in detrital allogenic sulphides; and(5) gold in secondary quartz veins. Uraninite is the principal uranium-bearing phase in the Witwatersrand conglomerates and usually occurs as rounded, apparently detrital grains that are almost always encapsulated within seams of bituminous material.

Authigenic uranium phases include brannerite and uraniferous leucoxene, both of which formed during post depositional stages of mineralization in the Basin. The petrographic studies of numerous authors (Liedenberg, 1955; Ramdohr, 1958; Feather and Koen, 1975) have shown that the mineralized conglomerates consist of both allogenic and authigenic minerals, with the result that the modified placer theory is now widely accepted as the most accurate representation of Witwatersrand ore genesis. Mineralization in the Witwatersrand Basin is now recognized as defining a distinct paragenetic sequence which formed in response to the successive increments of burial and metamorphism of the deposit at ca. 2550 Ma, 2350 Ma and 2050 Ma (Robb et al., 1997).

Evander Goldfield

Located in the easternmost extremity of the Witwatersrand Basin (Fig. 1), the Evander Goldfield is separated from the main basin by basement highs which comprise both granite and greenstone remnants (Hirdes, 1979; Ferraz et al., 1986). Greenstone belts, possibly correlatable with extensions of those in the Barberton region, represent an unusually high proportion of the basement terrane beneath and to the east of the Evander Goldfield.

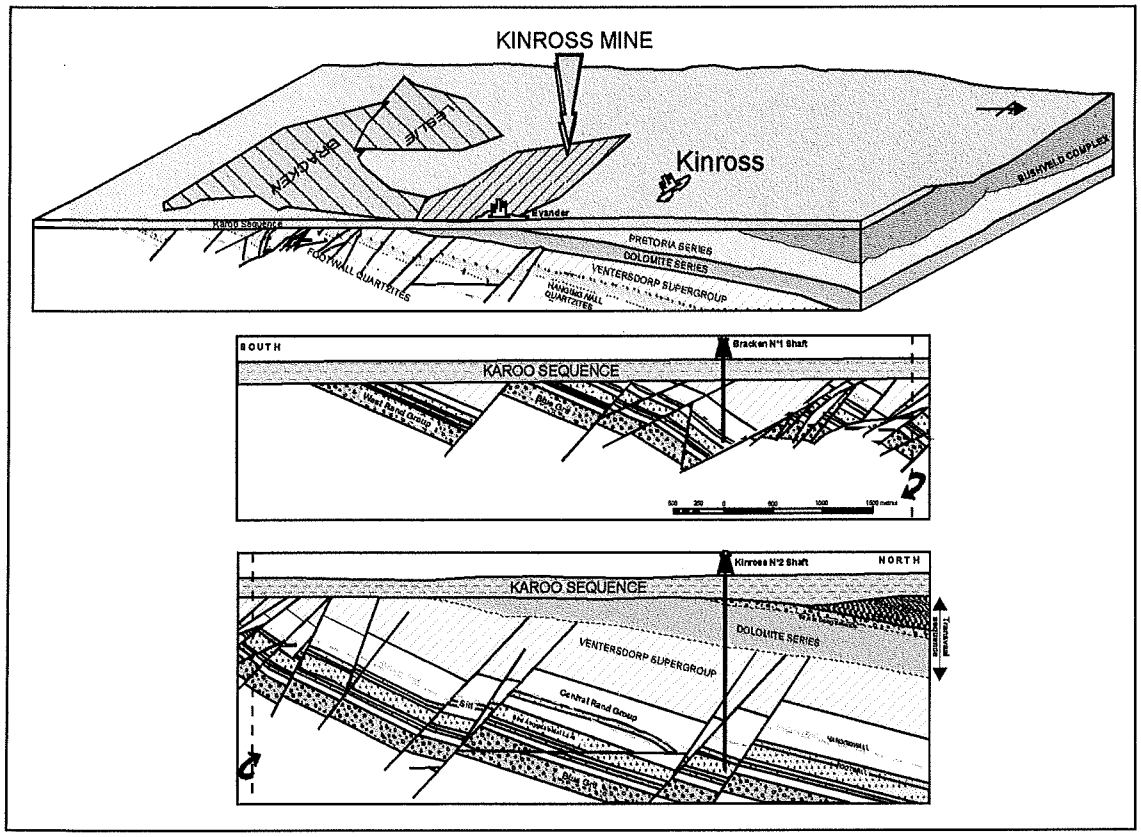

Figure 2 : Block diagram and dip sections of the Evander Goldfield.

Gold is extracted from 4 mines in the Evander Goldfield (Fig. 2), namely the Bracken, Winkelhaak, Leslie and Kinross mines. The Kimberley Reef, located towards the base of the Turffontein Subgroup of the Central Rand Group (Fig. 3), is the only gold-producing horizon within the Evander Basin. Other conglomeratic horizons do carry gold values, but too sporadically to warrant economic exploitation (Tweedie, 1986). The Kimberley Reef comprises a composite sequence of fluvial, channel-sediments, which was deposited on a regular palaeosurface striking northwest-southeast and dipping to the northeast. This low-grade placer is thickest in the southeast and thins rapidly in a west to north-west direction. According to Tweedie (1986), the Kimberley Reef represents the distal facies of a fluvial placer. The very high chromite/zircon ratios, as well as

the abnormally high platinium group element contents in the conglomerate, suggest an abnormally high proportion of mafic material (probably Archaean greenstone belts) in the sediment source area (Hirdes, 1979; Ferraz et al., 1986).

The Witwatersrand sediments in the Evander Basin comprise a sequence that is both more attenuated and different to strata elsewhere in the Basin. For the West Rand Group, which is only 750m thick in the Evander region, sequences correlatable with the Jeppestown Subgroup are missing. The Hospital Hill Subgroup is highly attenuated and characterized by interbedded shales and quartzites, while the Government Subgroup comprises an interbedded sequence of shales, siltstones, quartzites and polymictic greywackes (Fig. 3). The Central Rand Group comprises a composite sequence of interbedded conglomerates and quartz-wackes, with an average thickness of only 650m, compared to over 2000m elsewhere in the Witwatersrand Basin. The contact between the upper portion of the Central Rand Group and the lavas of the Klipriviersberg Group appears to be conformable (Tweedie, 1986). These lavas are, in turn, overlain by rocks of the Transvaal and Karoo Supergroups.

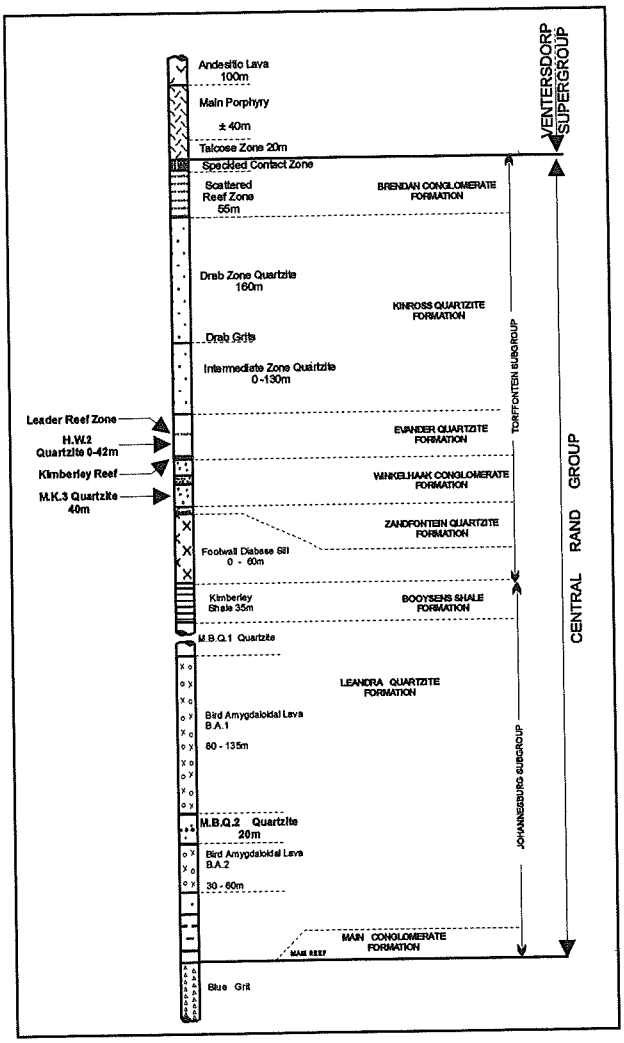

***Figure 3** : Stratigraphic column and sample locations.*

As shown by the dip sections in Figure 2, the Basin has undergone extensive faulting and reef duplication (Palmer et al., 1986). Three types of intrusion, which often occupy the major faults, are described within the Evander Goldfield and these may be linked to recognizable regional events:

(1) dolerite dykes related to outpouring of the Ventersdorp lavas;

(2) medium-to fine grained ophitic diabase dykes and sills related to the Bushveld event; and

(3) dolerite dykes related to the Karoo event.

A final feature that is specifically characteristic of the Evander Basin is the presence of a prominent aureole of contact metamorphism which is attributable to the close proximity of the Bethal lobe of the Bushveld Complex (Fig. 2). This metamorphism has affected the Witwatersrand sediments both on local (concentric zoning within individual pebbles) and regional (fluids focused along the contacts of shale horizons) scales (Tweedie, 1986). The highest metamorphic grades fall within the hornblende-hornfels facies.

SAMPLING

Two samples were collected within the Kimberley Reef footwall at Kinross Mine (Fig. 3), namely the Main Bird Quartzite (MBQ2) from the Leandra Quartzite Formation (Johannesburg Subgroup) and the Main Kimberley Quartzite (MK3) from the Winkelhaak Conglomerate Formation (Turffontein Subgroup). The Kimberley Reef was sampled at different locations within the Kinross Mine; sample KIN 94-2a was taken from an undeformed zone, samples KIN 95 - 2, 3, 4 were

obtained from shear zones cutting through the Kimberley Reef, and samples KIN 95- 5 and 6 were taken from sheared bitumen-rich zones. Two samples were collected from the upper part of the Turffontein Subgroup, within the Evander Quartzite Formation, namely, the Hanging Wall Quartzite (HW2) and the overlying Leader Reef.

ANALYTICAL METHODS

Single Zircon Grain Analysis

Zircons were separated from the rocks using a Wilfley table and a Frantz isodynamic separator. Pure zircon fractions were examined with a binocular microscope and by scanning electron microscopy in order to assess grain quality, degree of fracturing and the possible existence of inherited cores. No zircons were observed with identifiable cores and badly fractured or altered grains were ignored. Most grains were characterized by subrounded morphologies and surface textures consistent with mechanical transport and abrasion. A smaller proportion of grains, however, had euhedral or subhedral outlines and their origin could not be determined unequivocally. A selection of such grains was included in this study in order to assess the possibility that they might be authigenic.

Carefully handpicked zircons were washed with ultrapure diluted nitric acid, abraded using the techniques of Krogh (1982), weighed on a Cahn micro-balance and then chemically processed without separating U and Pb (Lancelot et al., 1976). An aliquot of the resulting solution was extracted and mixed with a ^{208}Pb-^{235}U spike for determination of Pb and U concentrations; an unspiked aliquot was used for measurement of Pb isotopic compositions. Analyses were carried out on a rhenium filament and the solution was co-precipated with a 0.25 N H_3PO_4--Silicagel mixture.

Pyrite Analysis

Pyrites were extracted from the samples using the techniques described above. The fractions were carefully selected under binocular microscope, washed in acetone and dissolved in a Savilex™ beaker with Aqua-Regea and a few drops of HBr. Lead was separated and purified on ion exchange resin (Bio Rad AG 1x8) with 0.5 N HBr and an elution using 6N HCl. Lead and uranium concentrations were determined from a spiked aliquot (^{207}Pb-^{235}U spike). Lead was loaded onto a Re filament with H_3PO_4 and Silicagel whereas uranium was anaysed on a W filament with $TaCl_5$.

The isotopic ratios were measured on a VG Sector Mass Spectrometer, corrected by 0.002 (± 0.05%) for mass fractionation. Data were reduced using PbDat (Ludwig, 1993a). Analytical uncertainties are listed at 2σ. Age determinations were processed using Isoplot (Ludwig, 1993b).

RESULTS

U-Pb Isotopic Data on Zircon Grains

A total of 67 single zircon grains were analyzed. Sample weights vary from 2 to 11 micrograms. Uranium and lead contents vary markedly, ranging from 6 to 1200 ppm and 5 to 570 ppm respectively. Data points for each stratigraphic level sampled are plotted on 5 different concordia diagrams (Fig. 4 A to E), while the U-Pb isotopic data are listed in Table 1. The degree of discordance of more than 60% of the grains plotted on the concordia diagrams is less than 10%. Only isotopic ratios that are less than 10% discordant were considered as reliable indicators of age. As analyses of individual detrital grains record age information about the zircon-bearing source rocks that contributed to the sediment (Barton et al., 1989; Bruguier, 1996; Robb et al., 1990), the ages of

these grains are discussed in terms of their $^{207}Pb/^{206}Pb$ ages which provide minimum estimates of the age of rock which furnished the grain. The zircon grains were carefully selected so that no visible signs of inheritance were present, thereby minimizing the possibility that inheritance has affected the age determination. With the exception of grains 36 and 39 from sample KIN 95-3, all the grains with uranium concentrations less than 100 ppm are all less than 10% discordant. As all the samples were collected underground within the Kinross Mine, they are free of weathering effects and so the lead loss recorded in the discordant grains must be related to some other phenomenon. Excessive (>30%) degrees of discordance have been recorded for zircons from the Barberton Mountain Land (Tegtmeyer and Kröner, 1987), as well as from Murchison Greenstone Belt (Poujol et al., 1996) where even gem-quality grains are discordant. It appears likely, therefore, that many of the discordant detrital grains in the Evander Basin might already have been discordant prior to their introduction into the depository.

Detrital Zircon Grains

Johannesburg Subgroup

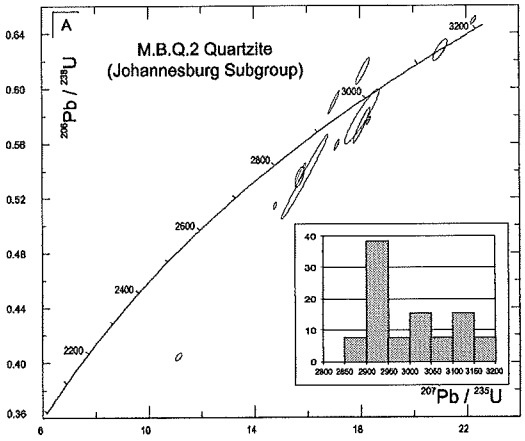

Figure 4 *: Concordia diagram, sample MBQ2.*

Fourteen zircon grains were analyzed from the Main Bird Quartzite (MBQ2) sample, all of which are detrital in origin. They span an age of 285 million years between 3179 and 2894 Ma, with a mean of 3008 Ma (Fig. 4). These data constrain the maximum depositional age for the Johannesburg Subgroup at 2894 Ma.

Turffontein Subgroup

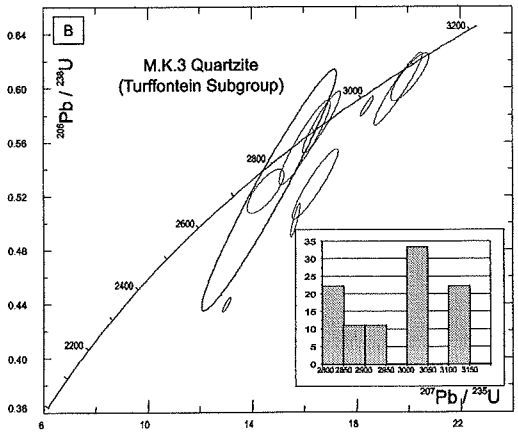

Figure 5 *: Concordia diagram, sample MK3.*

For the Main Kimberley Quartzite (MK3) ten detrital zircons were analyzed yielding ages which range between 3116 Ma and 2835 Ma. The mean is 2969 Ma (Fig. 5).

For the Kimberley Reef itself 29 grains were analyzed from 4 different locations (Fig. 6), not all of which are detrital. The most concordant points are those from the relatively unaltered and undeformed sample (KIN 94-2a) with ages ranging from 3115 Ma to 2771 Ma. Given that the age of the overlying Ventersdorp lavas is 2714 Ma (Armstrong et al., 1991), then all of the above grains would qualify as detritus. It is, therefore, tempting to suggest that the youngest zircon in this sample might reflect the maximum age of deposition of the Turffontein Subgroup. However, because there is still some doubt about the maximum age of the Ventersdorp lavas, the 2771 Ma zircon is not

regarded as a reliable indicator of the age of sediment deposition, and a more reliable indication of the maximum age of Turffontein Subgroup deposition is probably 2828 Ma (21; Table 1).

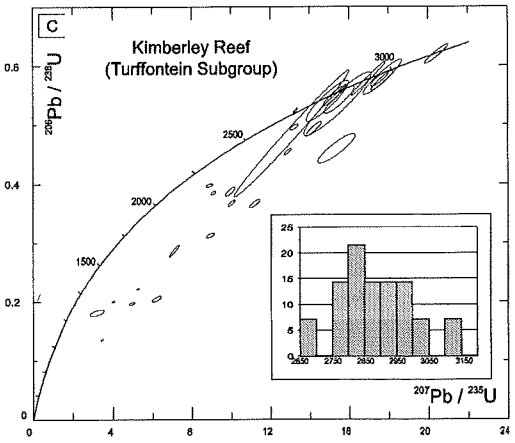

Figure 6 : Concordia diagram, sample Kimberley Reef.

It is pertinent to note that the three other samples of the Kimberley Reef, which are more intensely altered and deformed, show variable degrees of discordance (sometimes up to 70%) such that the resulting age determinations are less reliable. Certain grains are clearly detrital and their ages are consistent with the ranges discussed previously for sample KIN 94-2a.

Finally, 14 grains from the Hangingwall Quartzite (HW2 and Leader Reef) were also analyzed (Fig. 7A and B). The least discordant points span 160 million years and range in age between 3039 and 2940 Ma (geometric mean of 3008 Ma). Even for the discordant points, ages are older than the lower stratigraphic levels of the Central Rand Group and the geometric mean of this data set is identical to that of the MBQ2 sample.

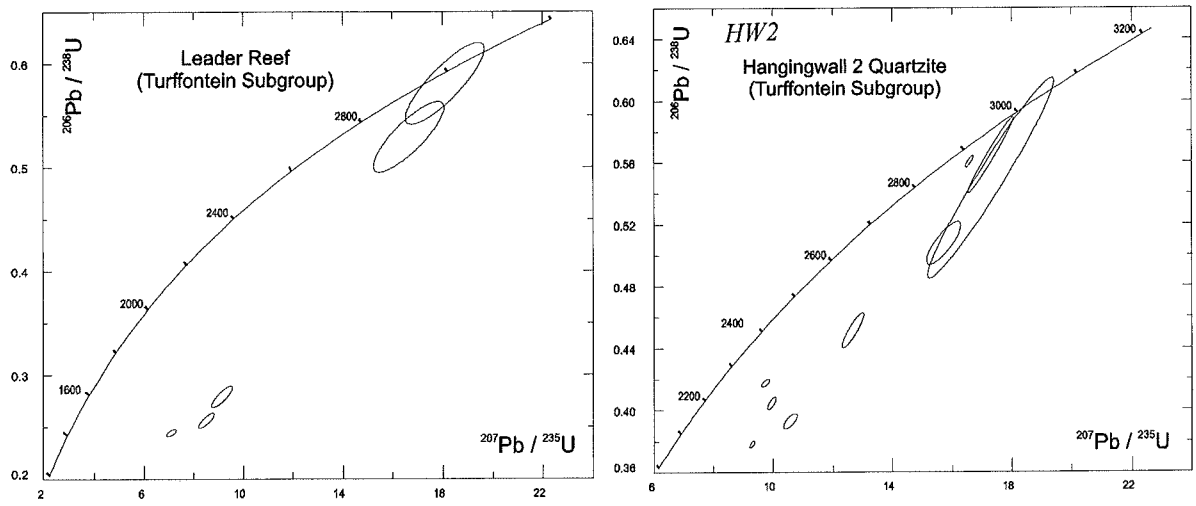

Figure 7 : Concordia diagrams, samples HW2 & Leader Reef.

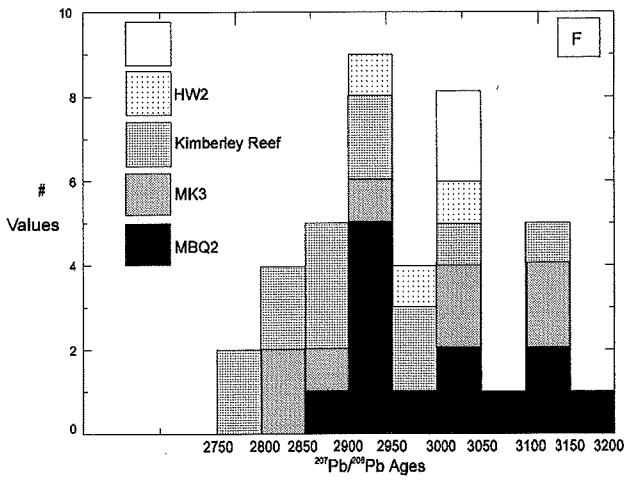

Figure 8 : Histogram of the $^{207}Pb/^{206}Pb$ ages for all the least discordant points.

The $^{207}Pb/^{206}Pb$ ages for all the least discordant detrital points (degree of discordance lower than 10%) from all the samples are summarized in the histogram of Figure 8. The mean age for the detrital zircon population analyzed from samples of the Central Rand Group collected in the Evander Goldfield is 2959 ± 34 Ma. This age is significantly younger than the mean 3053 Ma age found for the Central Rand Group in the other goldfields of the Witwatersrand Basin (Robb et al., 1990), and suggests that the source area was different.

Younger Zircons of Uncertain Origin

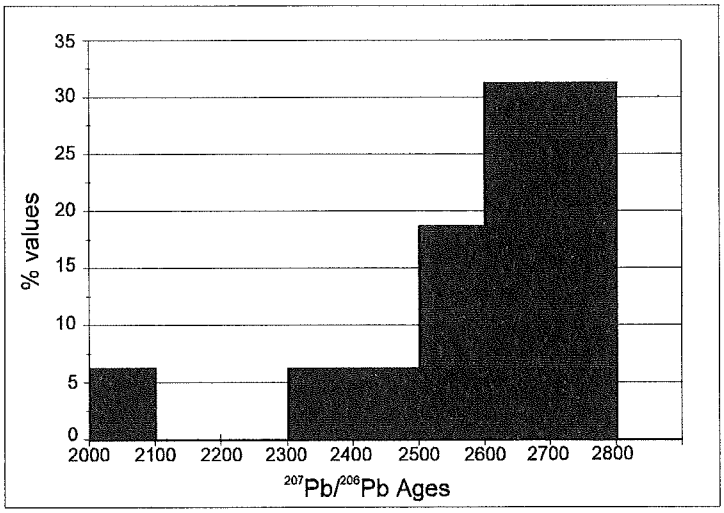

Figure 9 *: Histogram for zircons of uncertain origin.*

Examination of the data in Table 1 indicates that $^{207}Pb/^{206}Pb$ ages for zircons that are either well above or below the Kimberley Reef are consistent with a detrital origin for these grains. However, within the Kimberley Reef and its immediate hangingwall, and especially in material collected from shear zones cutting through the Kimberley Reef, a significant number (43%) of zircons yield ages that are younger or approximately equal to the age of the Ventersdorp lavas (i.e 2714 Ma). Many of these zircons also exhibit highly discordant $^{207}Pb/^{206}Pb$ ratios and should be regarded as age minima, although one of them (e.g. zircon 31, Table 1; 2690±5 Ma, -1% discordant) is concordant and represents a reliable age indicator. A compilation of these apparent ages (Fig. 9) indicates a broad range between ca. 2700 Ma and 2050 Ma. The majority of the apparent ages, however, including the concordant point, correspond broadly with the Ventersdorp event suggesting that these grains have been reset at this time; the remaining grains may have been wholly or partially reset at some other stage of the post-depositional history of the Basin. A previous study, for example (R. A. Armstrong, unpublished data quoted in Frimmel, 1994), has recognized authigenic zircon overgrowths dated at approximately 2580 Ma. It is, therefore, apparent that the U-Pb zircon data also reflect fluid circulation (and isotopic re-setting) during discrete events in the post-depositional history of the basin.

Table 1 : U-Pb data for zircons

Sample	Weight (mg)	U (ppm)	Pb (ppm)	$^{206}Pb/^{204}Pb$	$^{208}Pb/^{206}Pb$	$^{206}Pb/^{238}U$	$^{207}Pb/^{235}U$	$^{207}Pb/^{206}Pb$	apparent Age (Ma)	Disc. (%)
Leader Reef										
1 Zr, P, T	0.004	132	43	246	0.1058	0.2795 ± 3	9.131 ± 4	0.2369	3099 ± 32	48
2 Zr, P, T	0.0045	67	47	116	0.1435	0.5296 ± 5	16.662 ± 7	0.2282	3039 ± 62	10
3 Zr, P, T	0.0025	113	84	127	0.1480	0.5809 ± 5	18.098 ± 7	0.2259	3024 ± 61	2
4 Zr, P, D	0.0038	181	57	288	0.1637	0.2566 ± 2	8.511 ± 3	0.2405	3123 ± 26	53
5 Zr, P, D	0.0065	260	101	108	0.1494	0.2444 ± 1	7.070 ± 2	0.2098	2904 ± 27	51
HW2										
6 Zr, P, T	0.0072	22	15	251	0.1152	0.5475 ± 9	17.217 ± 10	0.2281	3039 ± 39	7
7 Zr, P, T	0.0048	89	62	489	0.1643	0.5648 ± 3	17.294 ± 3	0.2221	2996 ± 11	3
8 Zr, P, D	0.0050	149	105	254	0.3255	0.5079 ± 2	15.720 ± 3	0.2244	3013 ± 27	12
9 Zr, P, D	0.0050	646	276	842	0.0309	0.4046 ± 1	9.956 ± 1	0.1785	2637 ± 12	17
10 Zr, R, D	0.0093	535	228	826	0.0962	0.3782 ± .5	9.298 ± 1	0.1783	2637 ± 8	21
11 Zr, R, D	0.0112	463	295	762	0.0495	0.5606 ± .5	16.577 ± 1	0.2145	2940 ± 5	2
12 Zr, P, T	0.0030	254	140	302	0.1093	0.4515 ± 2	12.678 ± 2	0.2036	2856 ± 17	15
13 Zr, Y, T	0.0028	630	283	420	0.0864	0.3929 ± 1	10.569 ± 2	0.1951	2785 ± 20	23
14 Zr, Y, D	0.0086	712	329	684	0.0557	0.4176 ± .5	9.742 ± 1	0.1692	2550 ± 14	11
Kimb. Reef										
Kin 94-2a										
15 Zr, P, T	0.0068	31	18	202	0.0857	0.5347 ± 8	15.420 ± 9	0.2092	2899 ± 51	5
16 Zr, P, T	0.0037	118	75	257	0.0556	0.5418 ± 3	15.516 ± 4	0.2077	2887 ± 26	3

Table 1 Continued :

Sample	Weight (mg)	U (ppm)	Pb (ppm)	$^{206}Pb/^{204}Pb$	$^{208}Pb/^{206}Pb$	$^{206}Pb/^{238}U$	$^{207}Pb/^{235}U$	$^{207}Pb/^{206}Pb$	apparent Age (Ma)	Disc. (%)
17 Zr, P, D	0.0110	6	5	744	0.1358	0.6197 ± 2	20.448 ± 2	0.2393	3115 ± 11	0.2
18 Zr, P, D	0.0083	259	147	297	0.0085	0.4957 ± 1	13.221 ± 1	0.1934	2771 ± 13	6
19 Zr, P, T	0.0078	82	55	344	0.1395	0.5476 ± 2	15.211 ± 3	0.2015	2838 ± 18	0.8
20 Zr, R, T	0.0090	185	110	1205	0.3047	0.4542 ± 1	12.902 ± 1	0.2060	2875 ± 8	16
21 Zr, P, T	0.0045	65	43	174	0.0866	0.5395 ± 5	14.898 ± 6	0.2002	2828 ± 39	1.5
22 Zr, P, T	0.0030	121	91	200	0.1244	0.5801 ± 4	17.686 ± 4	0.2211	2989 ± 25	1
23 Zr, P, T	0.0059	275	181	1528	0.1448	0.5669 ± 1	15.861 ± 1	0.2029	2850 ± 7	-1
24 Zr, P, D	0.0036	182	124	415	0.1005	0.5747 ± 2	17.692 ± 2	0.2233	3004 ± 14	2.5
KIN 95-4										
25 Zr, P, T	0.0066	457	71	400	0.0862	0.1348 ± 1	3.476 ± 1	0.1870	2716 ± 16	70
26 Zr, P, T	0.0056	142	37	180	0.1210	0.2039 ± 2	6.213 ± 3	0.2210	2988 ± 33	60
27 Zr, P, D	0.0044	1077	243	457	0.1051	0.1995 ±.5	4.026 ± 1	0.1463	2304 ± 19	49
28 Zr, P, T	0.0040	202	113	678	0.1079	0.4927 ± 2	14.229 ± 2	0.2094	2901 ± 15	11
29 Zr, P, T	0.0046	1216	289	602	0.0314	0.2212 ±.5	5.288 ± 1	0.1733	2590 ± 12	50
KIN 95-3										
30 Zr, P, T	0.0056	889	401	252	0.0628	0.3964 ± .5	8.881 ± 1	0.1625	2482 ± 22	13
31 Zr, P, T	0.0086	490	288	2561	0.1155	0.5239 ± .5	13.299 ± .5	0.1841	2690 ± 5	-1
32 Zr, P, T	0.0104	73	62	551	0.1701	0.5774 ± 2	17.566 ± 2	0.2206	2985 ± 15	1.5
33 Zr, P, T	0.0088	245	105	1414	0.1378	0.3667 ± 1	10.038 ± 1	0.1985	2814 ± 12	28
34 Zr, P, T	0.0059	550	234	720	0.0849	0.3841 ± 1	9.115 ± 1	0.1721	2578 ± 13	18
35 Zr, P, T	0.0068	547	392	466	0.1225	0.5781 ± 4	16.984 ± 4	0.2131	2929 ± 10	0.5
36 Zr, P, T	0.0096	79	15	180	0.0218	0.1803 ± 2	3.213 ± 9	0.1292	2088 ± 99	48
37 Zr, P, T	0.0032	301	139	407	0.1375	0.3864 ± 1	9.967 ± 2	0.1871	2717 ± 18	22
38 Zr, P, T	0.0050	215	94	524	0.1388	0.3661 ± 1	11.221 ± 2	0.2223	2998 ± 16	33
39 Zr, P, T	0.0060	63	35	554	0.1248	0.4594 ± 4	15.385 ± 5	0.2428	3139 ± 36	22
KIN 95-2										
40 Zr, P, D	0.0090	11	5	173	0.1410	0.4847 ±18	13.106 ± 18	0.1961	2794 ± 64	8
41 Zr, R, D	0.0090	477	120	260	0.0995	0.2859 ± 3	7.127± 3	0.1808	2660 ± 20	39
42 Zr, P, D	0.0062	400	67	150	0.0178	0.1961 ± 1	4.989 ± 2	0.1845	2694 ± 52	57
43 Zr, P, D	0.0060	326	95	144	0.0269	0.3120 ± 1	8.963 ± 2	0.2084	2893 ± 38	39
MK3										
44 Zr, P, T	0.0070	95	74	236	0.1558	0.6082 ± 2	20.081 ± 3	0.2395	3116 ± 25	2
45 Zr, P, T	0.0110	144	97	1459	0.1032	0.5864 ± 1	18.410 ± 1	0.2277	3036 ± 6	2
46 Zr, P, T	0.0042	99	75	295	0.1664	0.5992 ± 3	19.620 ± 4	0.2374	3103 ± 19	2.5
47 Zr, P, T	0.0052	90	60	370	0.1174	0.5743 ± 3	16.667 ± 3	0.2105	2909 ± 21	0.5
48 Zr, P, T	0.0044	86	55	278	0.1314	0.5284 ± 4	16.418 ± 4	0.2253	3019 ± 26	9
49 Zr,Y, T	0.0022	49	32	147	0.0850	0.5245 ±14	14.649 ± 14	0.2025	2847 ± 58	4.5
50 Zr, P, T	0.0039	85	58	227	0.1019	0.5594 ± 4	16.025 ± 5	0.2077	2888 ± 31	1
51 Zr, P, T	0.0064	227	135	747	0.3213	0.4395 ± 1	13.010 ± 1	0.2147	2941 ± 9	20
52 Zr, P, T	0.0032	201	143	125	00379	0.5233 ± 2	14.515 ± 4	0.2011	2835 ± 43	4
53 Zr, P, T	0.0040	209	144	454	0.3091	0.5018 ± 2	15.650 ± 2	0.2262	3025 ± 12	13
MBQ2										
54 Zr, P,T	0.0058	30	22	424	0.2486	0.5759 ± .5	18.304 ± .5	0.2305	3056 ± 3	4
55 Zr, P, T	0.0066	56	38	269	0.0865	0.5587 ± .5	17.123 ± .5	0.2222	2997 ± 5	4.5
56 Zr, P, T	0.0040	73	44	227	0.0829	0.5141 ± .5	14.796 ± .5	0.2087	2894 ± 10	7.5
57 Zr, P, T	0.0028	211	567	305	3.9982	0.5896 ± 1	17.021 ± 1	0.2094	2901 ± 5	-3
58 Zr, P, T	0.0022	81	56	212	0.1200	0.5371 ± 1	15.761 ± 1	0.2128	2926 ± 8	5
59 Zr, P, D	0.0088	63	51	389	0.1129	0.6493 ± .5	22.297 ± .5	0.2490	3179 ± 9	-1.5
60 Zr, P, T	0.0091	22	18	150	0.0974	0.6134 ± 1	18.113 ± 1	0.2141	2940 ± 9	-5

Table 1 continued :

Sample	Weight (mg)	U (ppm)	Pb (ppm)	$^{206}Pb/^{204}Pb$	$^{208}Pb/^{206}Pb$	$^{206}Pb/^{238}U$	$^{207}Pb/^{235}U$	$^{207}Pb/^{206}Pb$	apparent Age (Ma)	Disc. (%)
61 Zr, P, T	0.0030	56	35	100	0.1177	0.5360 ± 1	15.732 ± 1	0.2128	2928 ± 11	5
62 Zr, Y, T	0.0045	42	35	115	0.3268	0.5726 ± 2	18.059 ± 1	0.2287	3043 ± 20	4
63 Zr, Y, T	0.0040	121	126	100	0.2179	0.5799 ± 3	18.157 ± 3	0.2271	3029 ± 22	2
64 Zr, P, T	0.0067	106	108	143	0.2255	0.6283 ± 1	21.065 ± 1	0.2432	3141 ± 12	0
65 Zr, P, T	0.0078	250	152	148	0.0846	0.4041 ±.5	11.135 ± 1	0.1998	2822 ±16	22
66 Zr, P, T	0.0037	47	38	102	0.1199	0.5348 ± 4	15.920 ± 4	0.2159	2947 ± 35	6
67 Zr, P, T	0.0095	52	51	132	0.0754	0.6726 ± 1	22.355 ± 1	0.2411	3126 ± 18	-1

P = pink, R= red, Y = yellow, T = translucent, D = dark

Pyrite

Pyrite classification

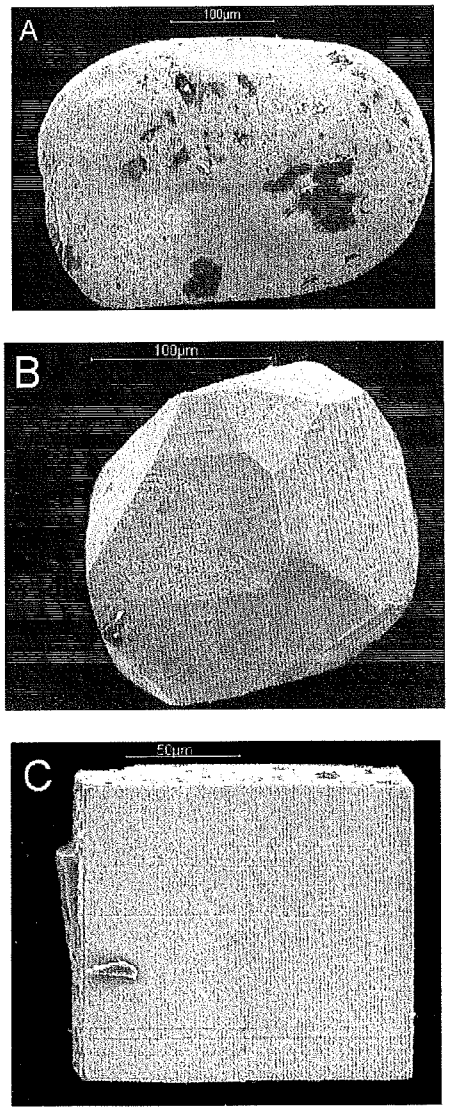

Figure 10 : *S.E.M. photographs of pyrite grains from Evander Goldfield samples.*

Within the Evander Goldfield, pyrite is by far the most abundant detrital heavy mineral, comprising 3 to 5 modal per cent of the conglomerate and often accounting for more than 90 per cent of the ore minerals (Tweedie, 1986; Hirdes, 1979; MacLean and Fleet, 1989). Several classification schemes for the Witwatersrand pyrites already exist, and the present study utilizes that of McLean and Fleet (1989), modified from Hallbauer's (1986) scheme, which recognized three basic textural types: (1) compact rounded allogenic/ detrital pyrite, (2) concretionary diagenetic pyrite and (3) idioblastic, authigenic pyrite associated with hydrothermal and/or metamorphic processes.

Two main pyrite types were identified within the Evander Goldfield (Fig. 10): round, compact crystals which are interpreted as detrital pyrites (Fig. 10A; Hallbauer, 1986; MacLean and Fleet, 1989), and idioblastic pyrites, which are either cubic, pyritohedral or octahedral in form (Fig 10B and C), interpreted as authigenic grains . The concretionary pyrite type was not identified in the present samples.

Results

Thirty-six fractions were analyzed from nine different samples. The isotopic results are listed in Table 2, and are plotted on Pb-Pb diagrams in Figure 11. The data show that with increasing stratigraphic height in the Central Rand Group, there is a general tendency for the proportion of authigenic pyrites to increase at the expense of detrital grains. Within the Kimberley Reef, less than 10 per cent of the pyrites appear to have detrital morphologies.

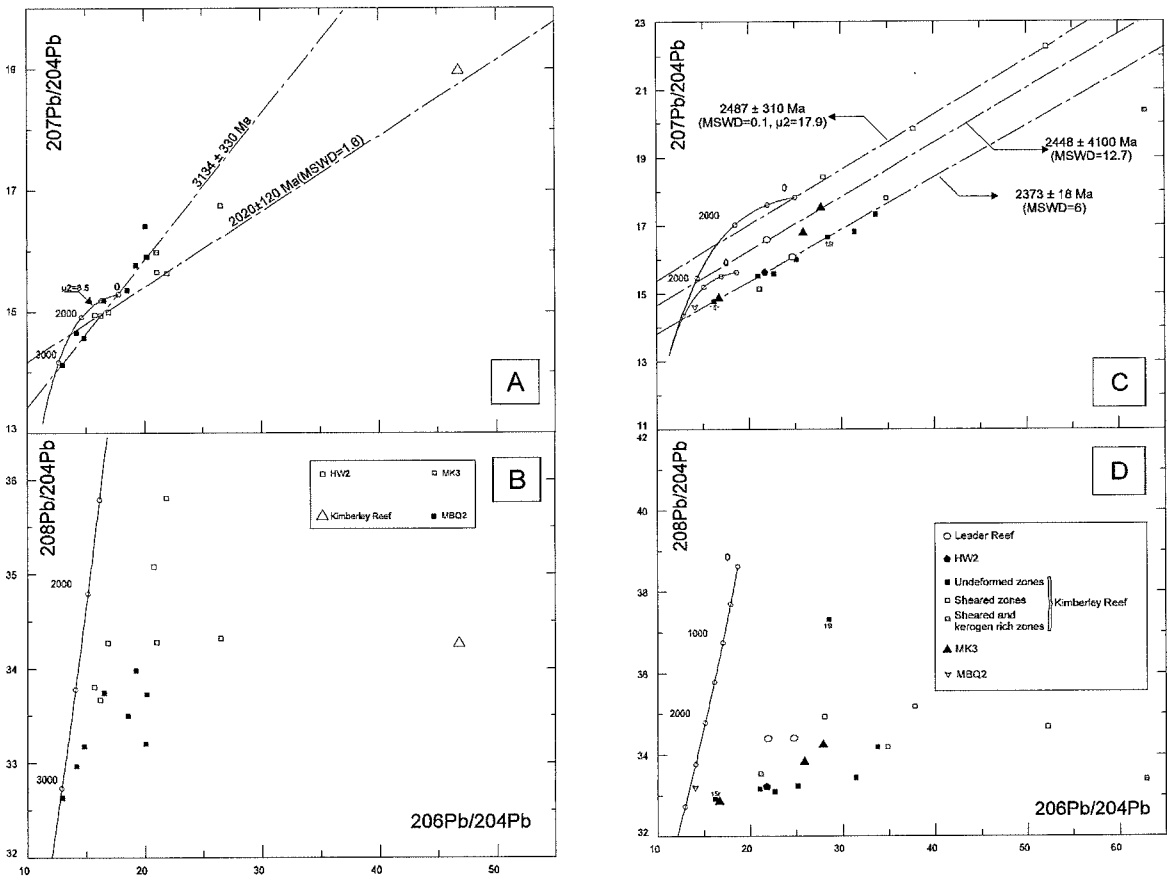

Figure 11: Pb-Pb diagrams for detrital grains (A and B) and euhdreal grains (C and D).

In the Pb-Pb diagrams all the isotopic ratios of detrital pyrites are shown in Figure 11 A and B. Isotopic ratios are seen to be very different from one sample to another. The less radiogenic signatures ($^{206}Pb/^{204}Pb$ between 12 and 20) were derived from pyrites within the M.B.Q.2 sample, located at the base of the Central Rand Group. These data (pyrites 29 to 36; Table 2) plot, with some scatter, along a secondary isochron which defines a poorly constrained age of 3134 ± 330 Ma and an initial μ_2 value of 8.5. For the H.W.2 quartzite, located in the Kimberley Reef hangingwall, the isotopic signature is again only weakly radiogenic ($^{206}Pb/^{204}Pb$ between 15 and 22) and these data (pyrites 6 to 9; Table 2) yield an age of 2020 ± 120 Ma (MSWD=1.6). For the other detrital fractions, from the Kimberley Reef and M.K.3 quartzite, the isotopic signatures are more radiogenic ($^{206}Pb/^{204}Pb$ up to 45 for the Kimberley Reef). These data (Fig. 11A) plot close to the two secondary isochrons previously defined. On the $^{208}Pb/^{204}Pb$ versus $^{206}Pb/^{204}Pb$ diagram (Fig. 11B), however, little or no correlation exists between uranium and thorium and there is no age significance to any of the data.

In the $^{207}Pb/^{204}Pb$ versus $^{206}Pb/^{204}Pb$ diagram for the euhedral pyrites (Fig. 11 C), it is again apparent that the isotopic signatures become more radiogenic with stratigraphic height. For example, some of the pyrite fractions display high U and Pb contents, reaching 120 and 198 ppm, respectively, for the sheared and bitumen-rich Kimberley Reef samples. If the lead isotope ratios of radiogenic lead derived from in-situ uranium decay are corrected, assuming that the uranium was incorporated at any time after the deposition of the Witwatersrand Basin, then all the recalculated model ages are too old for the time of formation of this pyrite. There is one exception, namely, the fraction Pyr 11 (Table 2). If it is considered that uranium has been incorporated at ~2.0 Ga, the recalculated isotopic composition for $^{206}Pb/^{204}Pb$=14.675 and for $^{207}Pb/^{204}Pb$=14.977, giving a model age of 2088 Ma and a μ value of 9.

Two fractions (Pyr 4 and 15 from the HW2 and Kimberley Reef samples, respectively), were subjected to acid leaching with diluted HCl and both the leached and residual phases were subsequently analysed for their Pb isotopic ratios (Table 2). It is apparent from this data that the leached fraction is far more radiogenic than the residue, suggesting that a stage of authigenic pyrite growth was associated with highly radiogenic fluids.

The data for the undeformed Kimberley Reef sample (Kin 94-2a) euhedral pyrites define a secondary isochron (slope=0.153) with a reasonably well-constrained age of 2380 ± 25 Ma (MSWD=6.6). In addition, samples Pyr 23, 17, 4 res and 1, plot on or close to this secondary isochron and together with the original data define a better-constrained age of 2373 ± 18 Ma (MSWD = 6). The remaining sample points define two other secondary isochrons, parallel to the one above, with poorly constrained slope ages of 2487 Ma for the sheared and bitumen-rich Kimberley Reef and 2448 Ma for the remaining points. In the $^{208}Pb/^{204}Pb$ versus $^{206}Pb/^{204}Pb$ diagram (Fig. 11 D) no correlation between uranium and thorium is observed, which is similar to the situation pertaining to the detrital pyrites (Fig. 11 B). Most of the points are again situated between the 3.0 and 2.0 Ga reference points.

The Pb-Pb isotope results from sulphide phases in the Evander Goldfield, confirm the existence of detrital pyrite whose age is ca. 3100 Ma, which is in a good agreement with the ages of the oldest detrital zircons from the MBQ2, Kimberley and Leader Reefs. In addition, at least two ages of crystallization of authigenic pyrite phases have been identified at ca 2370 and 2020 Ma. It is also evident that the majority of authigenic pyrite is restricted to the Kimberley Reef and its immediate footwall and hangingwall quartzites, suggesting that this was a zone of enhanced fluid flow and mineralization. The bitumen-rich zone appears to contain the highest concentrations of uranium and lead, which is consistent with the fact that hydrocarbons have preferentially accumulated around detrital lags of uraninite (Robb et al., 1997). It is also clear from leaching experiments that a more radiogenic lead isotope component is present on or near the pyrite surfaces, which suggests that post-depositional (possibly 2370 Ma) circulation of a highly radiogenic fluid took place.

Table 2 : Pb-Pb data for pyrite

Sample	$^{208}Pb/^{204}Pb$	$^{207}Pb/^{204}Pb$	$^{206}Pb/^{204}Pb$	Pb ppm	U ppm
Leader Reef					
Pyr 1 (*)	34.411	16.601	21.951	/	/
Pyr 2 (*)	34.418	16.073	24.754	24	7.8
HW2					
Pyr 3 (*)	39.239	26.573	245.279	/	/
Pyr 4 Leac (*)	41.848	45.076	270.374	/	/
Pyr 4 Res (*)	33.234	15.634	21.797	/	/
Pyr 5 (#)	33.803	14.937	15.718	/	/
Pyr 6 (#)	34.274	14.986	16.849	/	/
Pyr 7(#)	33.669	14.924	16.181	/	/
Pyr 8(#)	35.808	15.627	21.871	/	/
Pyr 9 (#)	35.079	15.694	20.760	/	/

Table 2 continued :

Sample	$^{208}Pb/^{204}Pb$	$^{207}Pb/^{204}Pb$	$^{206}Pb/^{204}Pb$	Pb ppm	U ppm
Kimberley Reef					
KIN 94-2a					
Pyr 10 (*)>200µ	33.445	16.816	31.256	40	39
Pyr 11 (*)<200µ	34.187	17.325	33.761	13	9
Pyr 12 (*)>200µ	33.243	16.005	25.130	/	/
Pyr 13 (*)	33.172	15.521	21.026	64	26
Pyr 14 (*)	33.103	15.592	22.649	71	nd
Pyr 15 Leac (*)	37.313	16.656	28.542	/	/
Pyr 15 Res (*)	32.920	14.775	16.253	/	/
Pyr 16 (#)	34.279	18.966	46.761	/	/
Gold	40.324	24.397	84.965	/	/
Kin 95-2					
Pyr 17 (*)	34.192	17.809	34.885	/	/
Pyr 18 (*)	34.684	22.267	52.201	/	/
KIN 95-4					
Pyr 19 (*)>100 µ	34.935	18.427	28.071	/	/
Pyr 20 (*)	35.179	19.844	37.794	/	/
Kin 95-5					
Pyr 21 (*)	33.538	15.144	21.148	198	120
Kin 95-6					
Pyr 22 (*)	33.397	20.371	62.937	197	35
MK3					
Pyr 23 (*)>200µ	32.876	14.860	16.717	/	/
Pyr 24 (*)<200µ	34.286	17.554	27.911	/	/
Pyr 25 (*)>200µ	33.867	16.833	25.959	/	/
Pyr 26 (#)>200µ	34.279	15.960	20.976	/	/
Pyr 27 (#)	34.321	16.729	26.509	/	/
MBQ2)					
Pyr 28 (*)	33.197	14.613	14.122	/	/
Pyr 29 (#)	33.742	15.168	16.530	/	/
Pyr 30 (#)	33.205	16.394	20.076	/	/
Pyr 31 (#)	33.728	15.884	20.181	/	/
Pyr 32 (#)	33.498	15.341	18.507	/	/
Pyr 33 (#)	33.981	15.755	19.261	/	/
Pyr 34 (#)	33.178	14.549	14.828	/	/
Pyr 35 (#)	32.632	14.108	12.981	/	/
Pyr 36 (#)	32.968	14.638	14.181	/	/

(*)=Euhedral Pyrites, (#)=Rounded Pyrites.

CONCLUSIONS

$^{207}Pb/^{206}Pb$ ages from detrital zircons in the Evander Basin exhibit a more restricted range of ages, which also exhibits a shift towards generally younger ages, than previously published data from the Central Rand Group (Fig. 12). The oldest grain measured in the present study is ca. 3180 Ma, whereas the majority of detritus falls in the range 3050 - 2850 Ma, with a mean age at ca. 2960 Ma. This mean is significantly younger than that obtained from the remainder of the Basin, which is approximately 3050 Ma. The Johannesburg Subgroup appears to have been deposited some time after 2890 Ma, the age of the youngest, unequivocally detrital zircon from the MBQ2. The suggestion by Tweedie (1986) that sediments below the Kimberley Reef were derived from a northeasterly source area whereas those above it were sourced from a different provenance to the southwest of the goldfield, is not supported by the present data which suggests that both packages of sediment contain detritus that is broadly similar in terms of its age range. The present study also confirmed the existence of detrital pyrite, characterized by compact, rounded morphologies and Pb-Pb isotopic ratios defining a secondary isochron at ca. 3100 Ma.

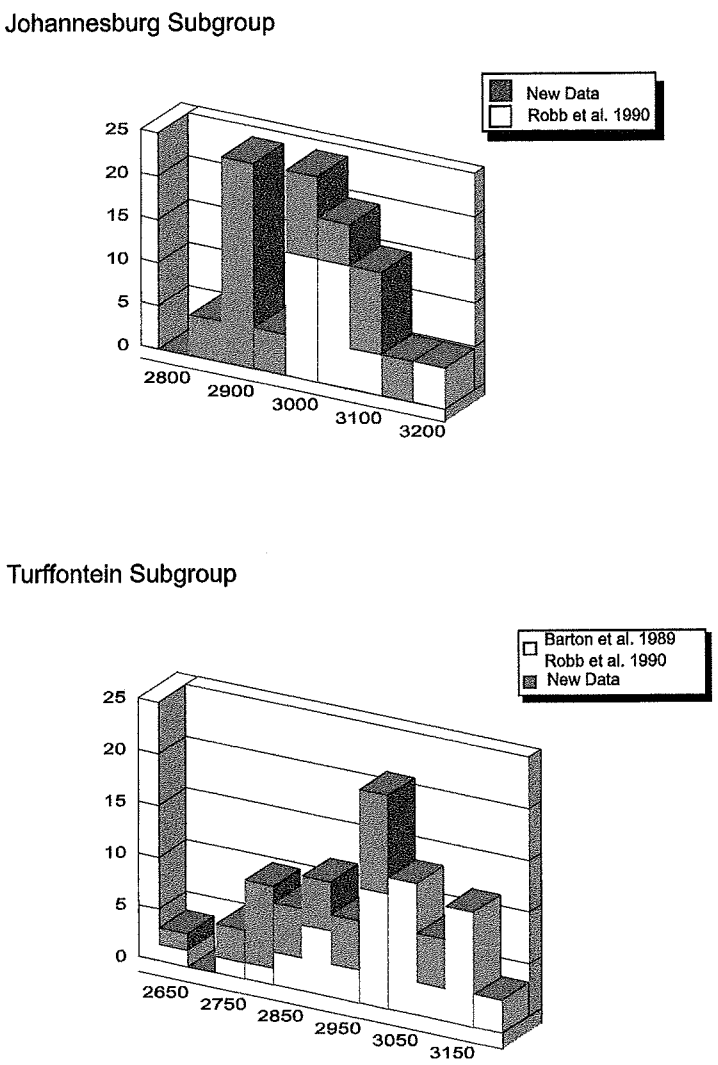

Figure 12 : Histogram of the $^{207}Pb/^{206}Pb$ ages.

$^{207}Pb/^{206}Pb$ data on zircons from the Kimberley Reef and its immediate hangingwall quartzite are characterized by a high proportion of apparent ages that are broadly similar to the minimum depositional age of the Witwatersrand Basin (2714 Ma) or are substantially younger than this limit. Most of these zircons have high U and Pb contents and also often exhibit relatively discordant $^{207}Pb/^{206}Pb$ ages which should, therefore, be regarded as minima. Isotopic re-setting of zircon appears to have been associated with deposition of the Ventersdorp lavas at ca. 2.7 Ga, as well as other discrete events during the post-depositional history of the Basin. In addition, a high proportion of authigenic pyrite grains in the Kimberley Reef, as well as other horizons in the Evander Basin, indicates that these rocks were also subjected to fluid circulation that resulted in substantial growth of new sulphide phases. A reasonably well-defined secondary isochron at 2370 Ma suggests that some authigenic pyrite grew during an event that may be related to burial of the Witwatersrand Basin by the upper portion of the Transvaal Supergroup (Robb et al., 1996). This interpretation must be treated with caution, however, as it is clear that pyrites exhibit a wide range of isotopic ratios that do

not fall on the 2370 Ma secondary isochron and could be the products of other episodic fluid-related events in the Witwatersrand Basin.

The zircon and pyrite grains that have been identified as having either authigenic morphologies and/or apparent ages that post-date Witwatersrand deposition, are characterized by high U contents (in the case of zircons) and highly radiogenic isotope ratios (in the case of pyrites). This is notably different from detrital zircon and pyrite which has significantly lower U contents and less radiogenic isotope ratios (Tables 1 and 2). In addition, a single analysis on an authigenic gold fraction from the Kimberley Reef also shows highly radiogenic isotopic ratios (Table 2). Thus, authigenic mineral growth in the interval 2.7 to 2.3 Ga appears to have taken place in the presence of a radiogenic fluid. However, the single zircon that yields an apparent $^{207}Pb/^{206}Pb$ age of 2090 Ma is characterized by a very low U content, while the detrital pyrites from HW2 which fall approximately on the 2020 Ma secondary isochron (Fig. 11A), are typified by low radiogenic isotope ratios. This suggests that the fluid associated with the late (ca. 2050 Ma) Bushveld related overprint in the Witwatersrand Basin was deficient in uranium. This observation needs to be substantiated by more data, but can tentatively be explained by the timing of bitumen precipitation with respect to the sequence of fluid flow events in the Basin. If, for example, bitumen was solidified around detrital uraninite lags at around 2350 Ma, as suggested by Robb et al. (1994; 1997), then fluids circulating through the Witwatersrand reefs subsequent to this event are unlikely to have interacted significantly with uraninite in the Basin and would consequently be depleted in labile uranium compared to fluids circulating prior to hydrocarbon generation.

The present study, which combines precise, single-grain, U-Pb dating of zircons with Pb-Pb isotopic studies of sulphide phases in the Evander Goldfield, has revealed a number of new observations which have considerable relevance to the genesis of the Au-U deposits of the Witwatersrand Basin. Although considerably more data is still required, these techniques appear to have the ability to distinguish between allogenic and authigenic components, as well as to recognize the timing of the paragenetic sequence in the Basin; these types of study may, therefore, contribute significantly to resolving the outstanding controversies that still exist with respect to Witwatersrand metallogenesis.

REFERENCES

Anhaeusser, C. R. and Burger, A. J., 1982. An interpretation of U-Pb zircon ages for Archaean tonalitic gneisses from the Johannesburg-Pretoria granite dome. Trans. Geol. Soc. S. Afr., 85: 111-116.

Antrobus, D.A., 1986. The goldfields of the Witwatersrand Basin. In: C. R. Anhaeusser and S. Maske (Editors), Mineral Deposits of Southern Africa, 1. Geological Society of South Africa, Johannesburg, pp. 489-493.

Armstrong, R. A., Compston, W., Retief, E. A., Williams, I. S. and Welke, H. J., 1991. Zircon ion microprobe studies bearing on the age and evolution of the Witwatersrand Triad. Precambrian Res., 53: 243-266.

Barton, E. S., Compston, W., Williams, I. S., Bristow, J. W., Hallbauer, D. T. and Smith, C. B., 1989. Provenance ages for the Witwatersrand Supergroup and the Ventersdorp Contact Reef : Contraints from ion microprobe U Pb ages of detrital zircons. Econ. Geol., 84: 2012-2019.

Bruguier, O., 1996. U-Pb ages on single detrital zircon grains from the Tasmieyle Group : implications for the evolution of the Olekma Block (Aldan Shield, Siberia). Precambrian Res., 78: 197-210.

De Wit, M. J., Roering, C., Hart, R. J., Armstrong, R. A., De Ronde, C. E. J., Green, R. W. E., Tredoux, M., Pederby, E. and Hart, R. A., 1992. Formation of an Archaean Continent. Nature, 357: 553-562.

Feather, C. E. and Koen, G. M., 1975. The mineralogy of the Witwatersrand reefs. Minerals Sci. Eng., 7: 189-224.

Ferraz, F. M., Robb, L. J. and Meyer, F. M., 1986. The nature of the Archaean basement in the provenance areas of the East Rand and Evander Goldfields (Abstr.). Geocongress '86, Johannesburg, pp. 115-118.

Frimmel, H.E. 1994. Metamorphism of the Witwatersrand gold. Exploration and Mining Geology, 3, 357-370.

Hallbauer, D. K., 1986. The mineralogy and geochemistry of Witwatersrand pyrite, gold, uranium, and carbonaceous matter. In: C. R. Anhaeusser and S. Maske (Editors), Mineral Deposits of Southern Africa, 1. Geological Society of South Africa, Johannesburg, pp. 731-752.

Hirdes, W., 1979. The Proterozoic gold-uranium Kimberley Reef placer in the Evander and East Rand Goldfields, Witwatersrand, South Africa-different facies and their source area aspects. Ph.D. Thesis, Heidelberg, 199 pp.

Jahn, B.M., Bertrand-Safarti J., Morin, N. And Mace, J., 1990. Direct dating of stromatolite carbonates from the Schmidtsdrift Formation (Transvaal Dolomite), South Africa, with implications on the age of the Ventersdorp Supergroup. Geology, 18, p. 1211-1214.

Krogh, T. E., 1982. Improved accuracy of U-Pb ages by the creation of more concordant systems using an air abrasion technique. Geochim. Cosmochim. Acta, 46: 617-649.

Lancelot, J., Vitrac, A. and Allegre, C. J., 1976. Uranium and lead isotopic dating with grain by grain zircon analysis : A study of complex geological history with a single rock. Earth Planet. Sci. Lett., 29: 357-366.

Liedenberg, W. R., 1955. The occurence and origin of gold and radioactive minerals in the Witwatersrand system, the Dominion Reef, the Ventersdorp Contact Reef and the Black Reef. Trans. Geol. Soc. S. Afr., 58: 101-254.

Ludwig, K.R., 1993a. A computer program for processing Pb-U-Th isotope data. U.S. Geol. Survey, Open File Rep., 88-542, 32 pp.

Ludwig, K.R., 1993b. A plotting and regression program for radiogenic-isotope data. U.S. Geol. Survey, Open File Rep., 91-445, 42 pp.

MacLean, P. J. and Fleet, M. E., 1989. Detrital pyrite in the Witwatersrand gold fields of South Africa: Evidence from truncated growth banding. Econ. Geol., 84: 2008-2011.

Minter, W.E.L., 1978. A sedimentological synthesis of placer gold, uranium and pyrite concentrations in Proterozoic Witwatersrand sediments. Mem. Can. Soc. Petrol. Geol., 5, 801-829.

Palmer, J. A., Phillips, G. N. and Mc Carthy, T. S., 1986. Do paleosols constrain oxygen levels during Witwatersrand deposition? (abstr.). Geocongress '86, Johannesburg, pp. 167-171.

Phillips, G. N., 1988. Widespread fluid infiltration during metamorphism of the Witwatersrand goldfields: Generation of chloritoid and pyrophyllite. J. Metamorphic Geol., 6: 311-332.

Poujol, M., Robb, L. J., Respaut, J. P. and Anhaeusser, C. R., 1996. 3.07-2.97 Ga greenstone belt formation in the northeastern Kaapvaal Craton : Implications for the origin of the Witwatersrand Basin. Econ. Geol., 91, 1455-1461.

Pretorius, D.A., 1991. The sources of Witwatersrand gold and uranium: A continued difference of opinion. Econ. Geol., Monograph 8, 139-163.

Ramdohr, P., 1958. New observations on the ores of the Witwatersrand in South Africa and their genetic significance. Trans. Geol. Soc. South Africa, 61: 1-50.

Robb, L. J. and Meyer, F. M., 1990. The nature of the Witwatersrand hinterland : Conjectures on the source area problem. Econ. Geol., 85: 511-536.

Robb, L. J., Davis, D. W. and Kamo, L., 1990. U-Pb ages on single grain detrital zircon grains from the Witwarersrand basin, South Africa : Constraints on the age of sedimentation and the evolution of granites adjacent to the Basin. J. Geol., 98: 311-328.

Robb, L.J., Landais, P., Meyer, F.M., Davis, D.W., 1994. Nodular organic matter in granites : implications for the origin of "kerogen" in the Witwatersrand Basin, South Africa. Exploration Mining Geology, 3, 219-230.

Robb, L. J. and Meyer, F. M., 1994. Geological environment and mineralization processes during the formation of the Witwatersrand Au-U deposits (Abstr.). XVth CMMI Congress, Johannesburg, pp. 3-18.

Robb, L. J., Charlesworth, E.G.., Drennan, G.R.., Gibson, R.L. and Tongu, E.L., 1997. Tectono-metamorphic setting and paragenetic sequence of Au-U mineralisation in the Archaean Witwatersrand Basin, South Africa. Austr. J. Earth Sci., 44, 353-371.

Skinner, B. J. and Merewether, P., 1986. Genesis of the Witwatersrand ores: Evidence versus prejudices (Abstr.). Geocongress '86, Johannesburg, pp. 81-83.

Tegtmeyer, A. R. and Kröner, A., 1987. U-Pb zircon ages bearing on the nature of early Archean greenstone belt evolution, Barberton Mountain Land, southern Africa. Econ. Geol., 36: 1-20.

Tweedie, E. B., 1986. The Evander Goldfield. In: C. R. Anhaeusser and S. Maske (Editors), Mineral Deposits of Southern Africa, 1. Geological Society of South Africa. pp. 705-730.

Wallmach, T. and Meyer, F. M., 1990. A petrogenetic grid for metamorphosed aluminous Witwatersrand shales. S. Afr. J. Geol., 93: 93-102.

Watchorn, M.B. and O'Brien, M.F., 1991. The significance of marine modification in some Witwatersrand placers - an example from the lower Witwatersrand West Rand Group. S. Afr. J. Geol., 94, 5/6, 333-339.

Wronkiewicz, D.J. and Condie, K.C., 1987. Geochemistry of Archaean shales from the Witwatersrand Supergroup, South Africa: source area weathering and provenance. Geochim. Cosmochim. Acta, 51: 2401-2416.

__oOo__